Accepted Manuscript

Short-range versus long-range structure in $Cu(In,Ga)Se_2$, $Cu(In,Ga)_3Se_5$, and $Cu(In,Ga)_5Se_8$

Erik Haubold, Philipp Schöppe, Stefanie Eckner, Sebastian Lehmann, Ivan Colantoni, Francesco d'Acapito, Francesco di Benedetto, Susan Schorr, Claudia S. Schnohr

PII: S0925-8388(18)33692-2

DOI: 10.1016/j.jallcom.2018.10.026

Reference: JALCOM 47844

To appear in: *Journal of Alloys and Compounds*

Received Date: 22 May 2018

Revised Date: 1 October 2018

Accepted Date: 4 October 2018

Please cite this article as: E. Haubold, P. Schöppe, S. Eckner, S. Lehmann, I. Colantoni, F. d'Acapito, F. di Benedetto, S. Schorr, C.S. Schnohr, Short-range versus long-range structure in $Cu(In,Ga)Se_2$, $Cu(In,Ga)_3Se_5$, and $Cu(In,Ga)_5Se_8$, *Journal of Alloys and Compounds* (2018), doi: https://doi.org/10.1016/j.jallcom.2018.10.026.

This is a PDF file of an unedited manuscript that has been accepted for publication. As a service to our customers we are providing this early version of the manuscript. The manuscript will undergo copyediting, typesetting, and review of the resulting proof before it is published in its final form. Please note that during the production process errors may be discovered which could affect the content, and all legal disclaimers that apply to the journal pertain.

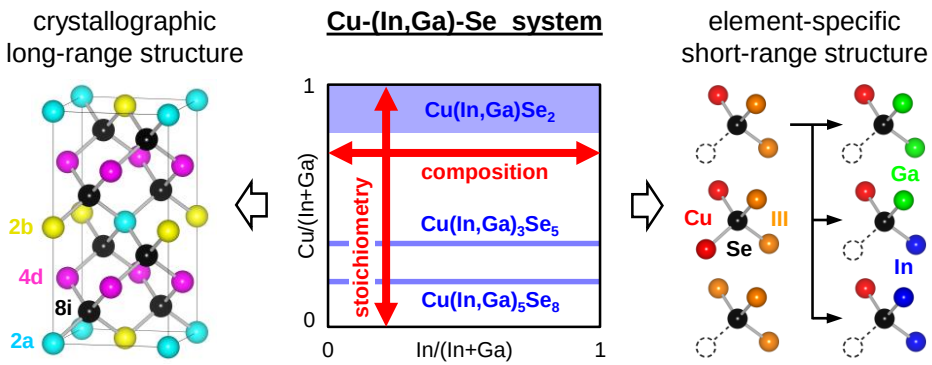
crystallographic
long-range structure
2b
4d
8i
2a
Cu-(In,Ga)-Se system
1
0
Cu/(In+Ga)
0
In/(In+Ga)
1
Cu(In,Ga)Se2
composition
Cu(In,Ga)3Se5
stoichiometry
Cu(In,Ga)5Se8
element-specific
short-range structure
Cu
III
Se
Ga
In

ACCEPTED MANUSCRIPT

Short-range versus long-range structure in $Cu(In,Ga)Se_2$, $Cu(In,Ga)_3Se_5$, and $Cu(In,Ga)_5Se_8$

Erik Haubold [a,1], Philipp Schöppe [a], Stefanie Eckner [a], Sebastian Lehmann [b,2], Ivan Colantoni [c,3], Francesco d'Acapito [c], Francesco di Benedetto [d], Susan Schorr [b,e] Claudia S. Schnohr [a,*]

[a] Institut für Festkörperphysik, Friedrich-Schiller-Universität Jena, Max-Wien-Platz 1, 07743 Jena, Germany

[b] Helmholtz-Zentrum Berlin für Materialien und Energie, Hahn-Meitner-Platz 1, 14109 Berlin, Germany

[c] CNR-IOM-OGG c/o ESRF LISA CRG, 71 Avenue des Martyrs, 38043 Grenoble, France

[d] Dipartimento di Scienze della Terra, Università degli Studi di Firenze, Via La Pira4, 50121 Firenze, Italy

[e] Institut für Geologische Wissenschaften, Freie Universität Berlin, Malteserstr. 74-100, 12249 Berlin, Germany

[1] Present address: IFW Dresden, Helmholtzstr. 20, 01069 Dresden, Germany

[2] Present address: Division of Solid State Physics and NanoLund, Lund University, 221 00 Lund, Sweden

[3] Present address: Dublin Institute for Advanced Studies, School of Cosmic Physics, Astronomy and Astrophysics Section, 31 Fitzwilliam Place, D02 XF86, Dublin, Ireland

* Corresponding author: PD Dr. Claudia S. Schnohr
Institut für Festkörperphysik
Friedrich-Schiller-Universität Jena
Max-Wien-Platz 1, 07743 Jena, Germany
c.schnohr@uni-jena.de

Abstract

The Cu-poor phases $Cu(In,Ga)_3Se_5$ and $Cu(In,Ga)_5Se_8$ play an important role both for understanding the Cu-(In,Ga)-Se material system and for growing high-efficiency $Cu(In,Ga)Se_2$ thin film solar cells. Using extended X-ray absorption fine structure spectroscopy, we have studied the element-specific short-range structure of $Cu(In,Ga)Se_2$, $Cu(In,Ga)_3Se_5$, and $Cu(In,Ga)_5Se_8$ alloys spanning the entire compositional range. The materials feature different local atomic arrangements and the element-specific average bond lengths remain nearly constant despite significant changes of the lattice constants with increasing In to Ga ratio and decreasing Cu content. In particular, the average bond lengths of Cu-Se and Ga-Se are almost identical while the average In-Se bond length is significantly longer in all three phases. The distance between lattice sites with mixed site occupation therefore corresponds to the weighted average of different element-specific bond lengths rather than to the individual bond lengths themselves. Furthermore, the increasing number of vacancies with decreasing Cu content lead to both a significant unit cell contraction and a slight bond length expansion. The crystallographic long-range structure and the element-specific short-range structure thus describe different structural aspects that are certainly interrelated but obviously not identical.

Keywords

semiconductors, atomic scale structure, EXAFS, synchrotron radiation, order-disorder effects, CIGS

ACCEPTED MANUSCRIPT

1. Introduction

Thin film solar cells with a $Cu(In,Ga)Se_2$ absorber prepared by co-evaporation have achieved a record efficiency of 22.6 % [1], thus closing the gap to silicon-based technologies. During a typical three-stage co-evaporation process, the absorber material evolves from $(In,Ga)_2Se_3$ to $Cu(In,Ga)_5Se_8$ (1-5-8 phase), then to $Cu(In,Ga)_3Se_5$ (1-3-5 phase), and finally to $Cu(In,Ga)Se_2$ (1-1-2 phase) [2,3]. The composition of the completed absorber layers is typically Cu-poor [1] but within the stability region of $0.8 \leq Cu/III = Cu/(In+Ga) \leq 1.0$ of the 1-1-2 phase [4,5]. Nevertheless, the $Cu(In,Ga)Se_2$ thin films may contain small precipitates of the 1-3-5 phase as probed by neutron diffraction measurements [6]. The fundamental understanding of the Cu-poor phases, $Cu(In,Ga)_5Se_8$ (Cu/III = 0.20) and $Cu(In,Ga)_3Se_5$ (Cu/III = 0.33), is thus important for the growth of high-efficiency $Cu(In,Ga)Se_2$ thin film solar cells.

The 1-1-2 phase crystallizes in the chalcopyrite type crystal structure (space group $I\bar{4}2d$) shown in Fig. 1 [7-10]. For the 1-3-5 phase, both a tetragonal structure with space group $P\bar{4}2c$ [11-13] and the stannite type crystal structure (space group $I\bar{4}2m$) [10,14-19] have been reported. Furthermore, the studies vary with respect to the occupation of the different cation sites within the stannite type structure shown in Fig. 1 [14,15,17]. For the 1-5-8 phase, both the tetragonal stannite type crystal structure [10,16,18-20] and a hexagonal crystal structure [13,19,20] were observed. Despite the differences between the various structures reported, especially regarding the long-range ordering of the cation sites, they all feature a tetrahedral coordination of both cation and anion sites. This is quite remarkable given that the number of cations is clearly smaller than the number of anions for the Cu-poor phases. Consequently, they feature a significant amount of cation vacancies and are also referred to as “vacancy phases”. Theoretical studies proposed a long-range ordering of vacancies and related defect pairs based on energy minimization [21,22]. While some contradicting results were obtained from previous experimental studies [24] more recent investigations using X-ray and neutron diffraction conclude that no evidence for long-range ordering of defects could be observed [10,17].

In the 1-3-5 and 1-5-8 phase, respectively, 20 and 25 % of the cation sites are vacant whereas the anion sites are fully occupied by Se. Thus, all cations are bound to four Se anions and the nearest neighbor environment of the cations does not change significantly with varying Cu content. This has been confirmed both experimentally and theoretically for the pure Cu-In-Se system with $0.2 \leq Cu/III \leq 1.0$ [18,22-26]. In contrast, the Se anions are surrounded by different nearest neighbor configurations, which can be classified by the number of valence electrons (κ): two Cu and two In or Ga atoms (κ = 8), one Cu atom, one vacancy, and two In

or Ga atoms (κ = 7), or one vacancy and three In or Ga atoms (κ = 9) as shown in Fig. 2 [14,22,27]. In the stoichiometric 1-1-2 phase, only the κ = 8 configuration occurs, whereas the 1-3-5 phase can be represented by 20 % κ = 8, 40 % κ = 7, and 40 % κ = 9 configurations. Similarly, the 1-5-8 phase corresponds to 50 % κ = 7 and 50 % κ = 9 configurations. The local environment of the Se anions therefore strongly depends on the Cu/III ratio, as confirmed for the pure Cu-In-Se system with $0.2 \leq Cu/III \leq 1.0$ [18,24,27]. Theoretical studies of pure Cu-In-Se compounds have further shown that for a given Cu content the difference in total energy of different crystal structures or polytypes is small as long as they feature the same local configurations [22,24,28,29]. The short-range structure is thus well-defined in terms of the different nearest neighbor configurations while the occupation and long-range ordering of the crystallographic cation sites may sensitively depend on the sample preparation and history, as indicated by the different crystal structures reported in the literature [24].

Interestingly, the Se atoms in $CuIn_3Se_5$ and $CuIn_5Se_8$ are displaced from the crystallographic lattice site depending on the specific cation configuration surrounding them [24]. The crystal structure thus represents the long-range average Se position but not the location of one particular Se atom. The same behavior was also observed for $Cu(In,Ga)Se_2$, where the mixed occupation of the group III lattice site with In and Ga atoms leads to different local cation configurations and thus to different Se displacements depending on the nearest neighbor environment [30,31]. This structural inhomogeneity on the subnanometer scale affects the local element-specific electronic states and the band gap energy of the material [30-32]. For the Cu-poor alloys $Cu(In,Ga)_3Se_5$ and $Cu(In,Ga)_5Se_8$, both the change in stoichiometry, i.e. the Cu/III ratio, and the change in composition, i.e. the In/III = In/(In+Ga) ratio, lead to an even larger variety of local cation configurations. Studying the short-range structure of these Cu-poor alloys is thus interesting also from a scientific point of view and provides a benchmark for theoretical calculations, which need to reproduce both the crystallographic long-range structure and the element-specific short-range structure to correctly predict the electronic properties of the material [32].

In this paper, we present a comprehensive study of $Cu(In,Ga)_3Se_5$ and $Cu(In,Ga)_5Se_8$ alloys spanning the entire compositional range. Element-specific bond lengths and bond length variations were determined by extended X-ray absorption fine structure spectroscopy (EXAFS). Comparison with our previous studies of $Cu(In,Ga)Se_2$ [30,33,34] provides a systematic investigation of the effects of both composition and stoichiometry on these local structural parameters. A significant difference between the crystallographic long-range structure and the element-specific short-range structure becomes evident, contributing to a

better understanding of the different structural features observed in these complex multinary material systems.

2. Experimental

2.1 Material synthesis

$Cu(In,Ga)_3Se_5$ powders spanning the entire compositional range of $0 \leq In/III \leq 1.0$ were synthesized by solid state reaction from the pure elements [16,17]. The reactions took place in evacuated silica glass tubes at a temperature of 1000°C with an excess of elemental selenium to prevent anion deficiency. Chemical and structural homogeneity were achieved by mechanical grinding and subsequent annealing at 650°C for five weeks. $Cu(In,Ga)_5Se_8$ powders also spanning the entire compositional range of $0 \leq In/III \leq 1.0$ were synthesized in a similar fashion. The material composition was determined by X-ray fluorescence analysis and inductively coupled-plasma mass spectrometry yielding the In/III and Cu/III ratios with an uncertainty of ± 0.02. For the 1-3-5 phase, the measured Cu/III ratios range from 0.31 to 0.37 with an average of 0.34 ± 0.02 in good agreement with the nominal value of 0.33. For the 1-5-8 phase, Cu/III ratios between 0.18 and 0.24 were measured with an average of 0.22 ± 0.02, again in good agreement with the nominal Cu/III ratio of 0.20. A qualitative phase analysis was performed by X-ray diffraction while detailed neutron diffraction and anomalous X-ray diffraction experiments provided the crystal structure, lattice constants, anion position, and site occupation factors [16,17]. The materials exhibit the stannite-type crystal structure over the whole compositional range but with mixed occupations of the cationic Wyckoff sites (see Fig. 1). Cu and vacancies are present at the 2a site while the 2b and 4d sites are occupied by Cu, Ga, and In. No evidence of long-range ordering of vacancies or defect complexes was observed and the lattice constants increase linearly with increasing In/III ratio in agreement with Vegard's Law.

The $Cu(In,Ga)Se_2$ powders with $0 \leq In/III \leq 1.0$ and $0.8 \leq Cu/III \leq 1.0$ studied previously were also synthesized by solid state reaction from the pure elements in a very similar manner [4,5,35] making them directly comparable to the $Cu(In,Ga)_3Se_5$ and $Cu(In,Ga)_5Se_8$ materials studied here. The 1-1-2 samples exhibit the chalcopyrite type crystal structure with Cu on the 4a site and Ga and In on the 4b site (see Fig. 1) and the lattice constants a and c also show a linear increase with increasing In/III ratio.

2.2 Measurements

Suitable samples for EXAFS transmission measurements were prepared by thoroughly grinding the powders together with cellulose in a ball mill. The mixture was then pressed into pellets with a diameter of 13 mm. The effective thickness of the pellets was chosen between one and two absorption lengths above the Cu and Ga K-edges for one set of samples and between one and two absorption lengths above the In K-edge for a second set of samples. Measurements of the Cu, Ga, and In K-edge were performed in transmission mode at the GILDA CRG beamline (BM08, now LISA) at the European Synchrotron (ESRF) in Grenoble, France [36]. The monochromator was equipped with Si(311) crystals. Mirrors with a Pd coating (E_{cutoff} ~ 18 keV) were used for the Cu and Ga K-edges and Pt coating (E_{cutoff} ~ 31 keV) was used for the In-K edge. The spectra were recorded at approximately 100 K to minimize thermal vibrations of the atoms. A reference foil or compound kept at room temperature in a second chamber was measured simultaneously to allow a precise alignment of the energy scales for different spectra.

The 1-1-2 samples studied previously were measured in transmission mode using BN-diluted powders pressed manually into suitable sample holders [30,33]. Spectra of the Cu, Ga, and In K-edge were recorded at a temperature of 17 K at Beamline C of HASYLAB (DESY) in Hamburg, Germany. In the framework of the present study, three 1-1-2 samples were prepared and measured at the ESRF in exactly the same way as the 1-3-5 and 1-5-8 samples to ensure the comparability of the measurements performed at different beamlines.

2.3 Data analysis

The data were processed and analyzed using the Ifeffit code [37] and the corresponding user interfaces Athena and Artemis [38]. After background subtraction, the spectra were Fourier transformed over a photoelectron wave number range of k = 3 – 14 $Å^{-1}$ using a Hanning window with a tapering parameter of dk = 2 $Å^{-1}$. The nearest neighbor scattering contribution was then fitted over a non-phase-corrected radial range of R = 1.4 – 2.9 Å for Cu and Ga and R = 1.5 – 3.0 Å for In, applying multiple k-weights of 2, 3, and 4. Phase shifts and scattering amplitudes were calculated using FEFF9 [39]. As mentioned above, the 1-1-2 phase crystallizes in the chalcopyrite type crystal structure whereas the 1-3-5 and 1-5-8 phases crystallize in a stannite type crystal structure with mixed occupation of the cation lattice sites (see Fig. 1). In contrast to X-ray or neutron diffraction, EXAFS is a very local probe and the details of the long-range ordering of the cations do not affect the nearest neighbor Se signal measured at the Cu, Ga, or In K-edge as long as the local coordination is similar. Therefore, a central cation absorber surrounded by four tetrahedrally bound Se nearest neighbors was

chosen as simplified structural model that is applicable to all cation edges and all phases studied. To check the validity of this approach, we also performed tests using structural models based on clusters of 35 atoms and a specific crystal structure, such as chalcopyrite or stannite. In all cases, we obtained the same relative differences for structural parameters determined for a given cation species and the absolute values remained within the experimental uncertainty. Furthermore, application of the simplified structural model to the EXAFS data of the 1-1-2 phase acquired previously reproduced the results reported in [30,33]. This clearly justifies the use of a common nearest neighbor model for all phases.

The coordination number was fixed to four throughout the fit since the cation to anion ratio is smaller than or equal to one for all phases and vacancies are expected predominantly on the cation lattice sites. A common amplitude reduction factor S_0^2 and threshold energy E_0 were set for all spectra measured at the same cation edge. Each bond species, such as Cu-Se, Ga-Se, and In-Se, exhibits a distance distribution rather than a single bond length due to thermal vibrations and static variations, the latter caused by different local configurations, defects, or strain. EXAFS probes this element-specific distance distribution, which is usually parameterized by the mean value R (average bond length), the standard deviation σ or variance σ^2 (bond length variation), and the asymmetry parameter C3 [40,41]. For temperatures well below room temperature, the distance distribution can be assumed to be Gaussian and, therefore, the asymmetry parameter was kept at zero throughout the analysis. Fitting the nearest neighbor scattering signal thus yields the element-specific average bond length R and bond length variation σ^2.

The magnitude of thermal vibrations increases with increasing temperature. This leads to an increase of the average bond length R and the bond length variation σ^2. Therefore, the structural parameters previously obtained for the 1-1-2 phase at 17 K [30,33] had to be adjusted to be comparable to the results obtained for the 1-3-5 and 1-5-8 phase at 100 K. A correction of $\Delta R_{thermal}$ = 0.002 or 0.001 Å was added to the average Cu-Se or Ga-Se and In-Se bond lengths, respectively. The values were derived from the difference in the average bond lengths of 1-1-2 samples measured previously at 17 K and room temperature together with the typical temperature dependence of the average bond length for tetrahedrally coordinated semiconductors [41]. The correction for the bond length variation was estimated using a correlated Einstein model [40,42] and amounts to $\Delta\sigma^2_{thermal}$ = 0.45, 0.13, and 0.18 x 10^{-3} Å^2 for Cu-Se, Ga-Se, and In-Se, respectively. The differences in the values, particularly for Cu-Se compared to Ga-Se and In-Se, stem from the different bond ionicity and the resulting

differences in bond strengths [30,31]. A small remaining difference between the σ^2 values of the 1-1-2 samples measured at ESRF and HASYLAB for both 100 K and room temperature most likely stems from the different sample preparation and beamline setup. It was therefore subtracted from all ESRF data to facilitate the comparability of the results. The overall uncertainties of the structural parameters were estimated by thoroughly testing all individual sources of uncertainty, including the choice of S_0^2 and E_0, data processing, parameter correlations in the fit, temperature corrections, and reproducibility. The resulting uncertainties varied for each source and absorption edge but were in almost all cases smaller than or equal to $\pm$ 0.003 Å and $\pm$ 0.3 x 10^{-3} Å^2 for the average bond lengths and bond length variations, respectively. For the sake of simplicity, these values were thus chosen as the overall uncertainty of the results derived from all spectra measured at the ESRF. For the 1-1-2 samples measured at HASYLAB, an overall uncertainty of $\pm$ 0.002 Å and $\pm$ 0.2 x 10^{-3} Å^2 for the average bond lengths and bond length variations, respectively, was previously estimated [33].

3. Results

3.1 Average bond lengths

The average Cu-Se, Ga-Se, and In-Se bond lengths R of $Cu(In,Ga)Se_2$, $Cu(In,Ga)_3Se_5$, and $Cu(In,Ga)_5Se_8$ are plotted as a function of composition in Fig. 3. For all three phases and all three types of bonds, the average bond lengths exhibit a small increase with increasing In/III ratio. The dependence is roughly linear and the slopes are similar within the experimental uncertainty for all phases and bonds. Furthermore, the average Cu-Se bond lengths systematically increase when going from the 1-1-2 to the 1-3-5 and then to the 1-5-8 phase. In contrast, the average Ga-Se and In-Se bond lengths are larger for the 1-3-5 phase than for the 1-1-2 phase but remain similar for the two Cu-poor phases.

3.2 Bond length variations

The Cu-Se, Ga-Se, and In-Se bond length variations σ^2 of $Cu(In,Ga)Se_2$, $Cu(In,Ga)_3Se_5$, and $Cu(In,Ga)_5Se_8$ are plotted as a function of composition in Fig. 4. There is no clear or pronounced dependence of the bond length variation on the In/III ratio within the experimental uncertainty for all phases and all types of bonds, in good agreement with previous observations for tetrahedrally coordinated III-V and II-VI ternary alloys [31]. Furthermore, the Cu-Se bond length variation exhibits only a small change with changing Cu content, being slightly higher for the Cu-poor phases than for the 1-1-2 phase. In contrast, the

Ga-Se and In-Se bond length variations show a pronounced and systematic increase when going from the 1-1-2 to the 1-3-5 and 1-5-8 phases. Note that for the 1-1-2 samples, the Cu/III ratio varies between 0.8 and 1.0, leading to a noticeable variation of the σ^2 values for Ga-Se and In-Se as discussed in Sect. 4.2.

4. Discussion

4.1 Dependence of the structural parameters on the composition

As already mentioned above, the lattice constants increase mostly linearly with increasing In/III ratio for each stoichiometry, namely 1-1-2, 1-3-5, and 1-5-8 [8-10,12,17,20,43]. However, the slope of this increase is different for a and c in all three phases. Therefore, the tetragonal distortion $\eta = c/2a$ also changes with changing In content. For the sake of simplicity, we thus consider an effective lattice constant a_{eff} defined as $V = a^2c = 2a_{eff}^3$, where V denotes the unit cell volume. Going from the pure Ga compound to the pure In compound, a_{eff} increases by almost 4 % for the 1-1-2 phase [8-10,43] and by about 5 % for the 1-3-5 and 1-5-8 phases [12,17,20] as shown in Fig. 5. The element-specific average bond lengths, plotted in Figs. 3 and 5, also exhibit a small increase with increasing In/III ratio that is similar for all types of bonds and phases. However, this change amounts to only 0.6 to 0.7 %, which is a factor 6 or 7 less than the change of the effective lattice constant. Consequently, the composition dependence of the element-specific average bond lengths clearly deviates from that of the unit cell volume.

Comparing $CuInSe_2$ with $CuGaSe_2$, the increase of the effective lattice constant is accompanied by a decrease of the relative Se position in x direction of approximately 0.025 [7,10]. The distance between the 4a (Cu) and 8d (Se) sites thus increases by less than 0.5 % while the distance between the 4b (In or Ga) and 8d sites increases by more than 7 %, in good agreement with the average Cu-Se, Ga-Se and In-Se bond lengths determined for $CuInSe_2$ and $CuGaSe_2$ by EXAFS [30,33]. The Se anion hence relaxes to a position that keeps the Cu-Se distance almost constant despite the change of the unit cell volume. In the mixed system $Cu(In,Ga)Se_2$, the distance between the 4a and 8d and between the 4b and 8d lattice sites changes continuously with In/III ratio from the $CuGaSe_2$ to the $CuInSe_2$ values [35]. Such a continuous change is indeed observed for the average Cu-Se bond length as determined by EXAFS measurements [30,33]. In contrast, the average Ga-Se and In-Se bond lengths are found to be very different from each other as shown in Fig. 5. Furthermore, they remain nearly constant over the entire compositional range changing by only one tenth of what would

be expected from the change of the 4b-8d lattice site distance. This behavior originates from the fact that bond stretching requires significantly more energy than bond bending [33]. As a consequence, the lattice mismatch in the alloy system is accommodated mostly by bond angle relaxation and only to a small extent by bond length relaxation. The Se anions thus relax to positions for which the element-specific distances remain close to those of the parent compounds. This characteristic behavior has been observed for numerous tetrahedrally coordinated semiconductor alloys [31] and demonstrates that the element-specific bond lengths generally differ from the distance

between the crystallographic lattice sites in materials with a mixed site occupation.

For $Cu(In,Ga)_3Se_5$, the lattice constants and anion position and thus the distances between the crystallographic lattice sites also change linearly with changing In/III ratio [17]. However, the relation between the crystal structure and the local atomic arrangements is even more complex for the 1-3-5 phase than for the 1-1-2 phase since the 2b and 4d sites of the stannite structure are occupied not only by Ga and In but also by Cu [17]. No anion position or site occupation factors have been reported for $Cu(In,Ga)_5Se_8$, but a behavior similar to that of the 1-3-5 phase may be expected. Nevertheless, the EXAFS results for the 1-3-5 and 1-5-8 phase plotted in Fig. 5 demonstrate that the average Ga-Se and In-Se bond lengths exhibit the same behavior as for the 1-1-2 phase. In particular, they are very different from each other and remain nearly constant over the entire compositional range despite the pronounced change of the unit cell volume. At the same time, the average Cu-Se and Ga-Se bond lengths are nearly identical for all three phases. This clearly demonstrates that the balance between bond length relaxation and bond angle relaxation is very similar for the 1-1-2, 1-3-5, and 1-5-8 phase and that the element-specific bond lengths remain close to their "natural" values independent of composition, stoichiometry, and site occupation. The Cu-poor phases $Cu(In,Ga)_3Se_5$ and $Cu(In,Ga)_5Se_8$ are thus characterized by strong bond angle distortions and severe atomic displacements leading to a structural inhomogeneity on the subnanometer scale. Similar to $Cu(In,Ga)Se_2$, this inhomogeneity can be expected to affect the band gap bowing and thus the electronic properties of the materials [30,31].

As discussed above, element-specific bond lengths and lattice site distances may differ strongly in materials with mixed site occupation. Nevertheless, they are intrinsically related. In fact, the distance between two lattice sites determined by diffraction equals the average of the element-specific bond lengths weighted by the site occupation factors for these elements on the particular lattice sites. In the present case, the 8d and 8i sites are always fully occupied by Se. For the 1-1-2 phase, the 4a site is populated solely by Cu such that $f^{4a}_{Cu} = 1$, where

f^{4a}_{Cu} denotes the fraction of 4a sites occupied by Cu. Therefore, the 4a-8d lattice site distance can be expressed as $R_{4a\text{-}8d} = f^{4a}_{Cu} R_{Cu\text{-}Se} = R_{Cu\text{-}Se}$ in agreement with previous studies [30]. The 4b site is populated randomly by Ga and In atoms such that f^{4b}_{In} = In/III = x and f^{4b}_{Ga} = 1-In/III = 1-x. The 4b-8d lattice site distance can thus be expressed as $R_{4b\text{-}8d} = f^{4b}_{Ga} R_{Ga\text{-}Se} + f^{4b}_{In} R_{In\text{-}Se} = (1\text{-}x) R_{Ga\text{-}Se} + x R_{In\text{-}Se}$, again in good agreement with previous studies [30].

For the 1-3-5 phase, neutron diffraction and anomalous X-ray diffraction measurements showed that 20 % of the 2a sites are occupied by Cu while the rest is vacant such that f^{2a}_{Cu} = 0.2 and f^{2a}_{Vac} = 0.8 [17]. Thus, $R_{2a\text{-}8i} = f^{2a}_{Cu} R_{Cu\text{-}Se} + f^{2a}_{Vac} R_{Vac\text{-}Se} = 0.2 R_{Cu\text{-}Se} + 0.8 R_{Vac\text{-}Se}$. As can be seen in Fig. 6, the distance between the 2a and 8i sites, calculated from the crystal structure parameters reported in [17], is significantly smaller than the average Cu-Se bond length determined by EXAFS. This can only be realized if the distance $R_{Vac\text{-}Se}$ between a vacant 2a site and the neighboring Se anions is significantly smaller than $R_{Cu\text{-}Se}$. The $R_{Vac\text{-}Se}$ values calculated from $R_{2a\text{-}8i}$ and $R_{Cu\text{-}Se}$ for the given site occupation are also plotted in Fig. 6. They are 6 to 7 % shorter than the average Cu-Se bond lengths. This is in excellent agreement with the experimental findings for pure $CuIn_3Se_5$ [15] and is intermediate to the predicted shortening of 3 and 10 % from theoretical calculations for pure Cu-In-Se compounds [22,44]. This clearly demonstrates the strong lattice relaxation around vacant 2a sites. The 2b and 4d sites are occupied by 20 % Cu and 80 % Ga or In such that $f^{2b/4d}_{Cu}$ = 0.2, $f^{2b/4d}_{Ga}$ = 0.8 (1-x), and $f^{2b/4d}_{In}$ = 0.8 x [17]. As shown in Fig. 6, the calculated distance between a cation site with these occupation factors and the 8i site, $R_{calc} = 0.2 R_{Cu\text{-}Se} + 0.8 (1\text{-}x) R_{Ga\text{-}Se} + 0.8 x R_{In\text{-}Se}$, agrees very well with the 2b-8i and 4d-8i distances calculated from the crystal structure parameters reported in [17]. In contrast, assuming a site occupation of 10 % Cu and 90 % Ga or In or of 30 % Cu and 70 % Ga or In yields a slope of the calculated lattice site distance with increasing In/III ratio that is clearly too steep or too flat, respectively (see Fig. 6). The comparison of the element-specific average bond lengths determined by EXAFS and the lattice site distances determined by neutron diffraction thus confirms the site occupation factors previously determined for $Cu(In,Ga)_3Se_5$. The combination of diffraction measurements and X-ray absorption spectroscopy therefore provides an alternative approach to determine site occupancies in multinary compounds and alloys.

4.2 Evolution of the structural parameters with changing stoichiometry

Going from $Cu(In,Ga)Se_2$ to $Cu(In,Ga)_3Se_5$ and $Cu(In,Ga)_5Se_8$, the stoichiometry changes from 1.00 ≥ Cu/III ≥ 0.80 to Cu/III = 0.33 and 0.20, respectively. This decrease in Cu content is accompanied by a decrease of the lattice constants a and c [10-17,20,35]. Similar to the

effect of changing composition discussed in Sect. 4.1, the two lattice constants decrease by different amounts such that the tetragonal distortion η also changes with varying Cu/III ratio. For the sake of simplicity, Fig. 7 therefore plots the change of the effective lattice constant $\delta a_{eff} = a_{eff}(Cu/III) - a_{eff}(Cu/III=1.00)$ for the pure Ga and In containing compounds. The decrease of a_{eff} with decreasing Cu/III ratio is already observed within the stability range of the 1-1-2 phase and continues to the 1-3-5 and 1-5-8 phases. Comparing the latter with the stoichiometric 1-1-2 phase, the effective lattice constant decreases by about 2 % for the Cu-Ga-Se system and by almost 1 % for the Cu-In-Se system. This significant contraction of the crystal structure is caused by the increasing number of vacancies, which occur on 20 and 25 % of the cation sites in the 1-3-5 and 1-5-8 phase, respectively. The number of atoms contained in the unit cell thus significantly decreases and, as a consequence, the lattice shrinks.

The element-specific average bond lengths determined from EXAFS measurements also exhibit a slight change with changing Cu/III ratio as described in Sect. 3.1. To evaluate this change with stoichiometry, a linear dependence of the bond lengths on the In/III ratio was assumed with the same slope for all atomic pairs and phases. The difference between the bond lengths of the different phases then becomes independent of the In/III ratio and can be expressed by $\delta R = R(Cu/III) - R(Cu/III=1.00)$. The values obtained for the Cu-Se, Ga-Se, and In-Se bond are plotted in Fig. 7. For the 1-1-2 phase, the Cu/III ratio of the samples varied between 0.80 and 1.00, however, no difference was observed for the element-specific bond lengths within the experimental uncertainty [30,33]. For the Cu-poor phases, the δR values increase for all three types of bonds corresponding to an expansion of the average bond lengths by 0.2 to 0.5 %. This change is one order of magnitude less than the change observed for the effective lattice constant. The element-specific average bond lengths thus remain nearly unchanged despite a significant reduction of the unit cell dimensions.

This behavior is again an expression of the strong tendency towards bond length conservation observed in all tetrahedrally coordinated semiconductors [31]. The energy of a given structure is dominated by the distortion energy associated with a change of the element-specific bond lengths. This has two important implications. Firstly, the system tries to minimize bond length distortions. Changes of the lattice dimensions due to a change of composition or stoichiometry are thus accommodated mostly by bond angle relaxation. Therefore, the Cu-poor alloys feature different anion displacements depending on the local atomic configurations rather than one unique anion position as suggested by the crystal structure [24,31]. Secondly, the energy of a given structure is dominated by nearest neighbor

interactions. Theoretical studies of Cu-In-Se compounds report that the differences in total energy between different crystal structures of a given stoichiometry are very small if the local atomic environments are similar [22,24,28,29]. Furthermore, nearest neighbor anion-cation clusters are found to be more stable than second nearest neighbor cation-cation clusters [29]. The short-range structure is thus well determined by the maxim of bond length conservation while the long-range order often depends on sample growth and history [24].

Previous studies of Cu-poor Cu-In-Se compounds reported an average Cu-Se bond lengths constant within the uncertainty of 0.005 Å [22,24] or an average Cu-Se bond lengths that is about 0.01 to 0.02 Å larger for the 1-3-5 and 1-5-8 phases than for the 1-1-2 phase [18,19, 23,25]. The change of the average In-Se bond lengths was mostly found to be within the uncertainty of about 0.005 Å [23,24,26] or 0.01 Å [22] and only one study reported a reduction of the average In-Se bond lengths by almost 0.02 Å for the 1-3-5 and 1-5-8 phase compared to the 1-1-2 phase [18]. No studies have been reported for Cu-poor Ga compounds or alloys.

The results presented in Fig. 7 are derived from an extensive set of samples with eight to ten different In/III ratios for each of the three different phases. The data clearly show a small increase of the bond lengths with decreasing Cu content by about 0.005 Å for Ga-Se and In-Se and by slightly more than 0.01 Å for Cu-Se. The behavior of the element-specific average bond lengths is thus opposite to that of the crystal lattice. This can again be understood by considering the significant amount of cation vacancies present in the Cu-poor phases. In the 1-3-5 and 1-5-8 phase, 80 and 100 % of the Se anions feature a neighboring cation vacancy, respectively [22,27]. The coordination number of the Se anions thus decreases from four in the 1-1-2 phase to only three in the 1-5-8 phase [18]. This reduced coordination leads to a weakening of the bonding and thus to an increase of the average bond lengths. Furthermore, the vacancies provide more space inside the structure. Together with the weakening of the bonds this facilitates atomic motion and hence thermal vibrations. Stronger vibrations of two neighboring atoms relative to each other could thus also contribute to the bond length expansion observed by EXAFS measurements [31,40-42].[1]

Interestingly, the bond length expansion seems to be slightly more pronounced for Cu-Se than for Ga-Se and In-Se. In the 1-1-2 phase, every Se atom is surrounded by two Cu and two In or Ga atoms corresponding to $\kappa = 8$ valence electrons. In the 1-5-8 phase, 50 % of the Se atoms

[1] Note that relative vibrations parallel to the bond direction affect the bond length variation but not the average bond length. In contrast, relative vibrations perpendicular to the bond direction do lead to an increase of the average bond length measured by EXAFS.

are surrounded by one Cu atom, one vacancy, and two In or Ga atoms ($\kappa = 7$) while the other 50 % of Se atoms are surrounded by one vacancy and three In or Ga atoms ($\kappa = 9$) [22]. In or Ga atoms are present in both configurations. Therefore, the nearest neighbor Se to an In or Ga atom has a 50 % chance to be in the $\kappa = 7$ configuration and a 50 % chance to be in the $\kappa = 9$ configurations. The average number of valence electrons for the Se atoms neighboring an In or Ga atom is thus still $\kappa = 8$, even though the coordination number is reduced to three. In contrast, Cu atoms are present only in the $\kappa = 7$ configuration. The number of valence electrons for Se atoms neighboring a Cu atom is therefore only $\kappa = 7$. Although all Se atoms in the 1-5-8 phase have a coordination of three, the Se atoms neighboring a Cu atom have a lower number of valence electrons and are thus more weakly bound than the average of the Se atoms neighboring an In or Ga atom. This could explain the more pronounced increase of the average Cu-Se bond length compared to the average In-Se and Ga-Se bond lengths apparent in Fig. 7. In conclusion, the large number of cation vacancies in the Cu-poor phases affects the short- and long-range structure in very different ways. While the unit cell volume significantly decreases, the element-specific average bond lengths slightly increase with decreasing Cu/III ratio.

This also has implications for the band gap energy of the material. Comparing the 1-5-8 phase to the stoichiometric 1-1-2 phase, the band gap increases by 0.2 to 0.3 eV and by 0.1 to 0.2 eV for the Cu-In-Se and Cu-Ga-Se system, respectively [12,19-22,24,26,29]. Considering only the crystal structure, one might be tempted to explain part of this increase by the decreasing unit cell volume, which would correspond to an increase of the band gap by approximately 0.05 and 0.2 eV based on the deformation potentials of $CuInSe_2$ and $CuGaSe_2$, respectively [45]. However, the interatomic distances do not decrease but remain nearly constant for all Cu/III ratios and thus the element-specific local electronic states do not change significantly either [32]. If anything, the slight bond length expansion by about 0.2 % would lead to a decrease of the band gap energy by roughly 0.01 and 0.02 eV for the Cu-In-Se and Cu-Ga-Se system, respectively. The increase of the band gap observed experimentally is therefore caused by a change of the stoichiometry rather than a change of the structural parameters. As discussed in [22], the decreasing Cu content leads to a weakening of Se *p* – Cu *d* interband repulsion and thus to a lowering of the valence band maximum and hence an increase of the band gap. This clearly demonstrates the importance of knowing both short- and long-range structural details in order to correctly interpret the electronic properties of the material.

The element-specific bond length variations are independent of the In/III ratio but vary significantly for the different phases, as described in Sect. 3.2. This is further demonstrated in

Fig. 8, which plots the Cu-Se, Ga-Se, and In-Se bond length variations σ^2 as a function of the Cu/III ratio. For the 1-1-2 phase, the data points for individual samples are plotted since the Cu/III ratio of these samples varies between 0.8 and 1.0 [33]. For the 1-3-5 and 1-5-8 phase, the Cu content is similar for all samples (see Sect. 2.1) and hence the average Cu/III ratio and bond length variation has been calculated for all samples of a given phase. The uncertainties represent the corresponding sample standard deviations.

For the 1-1-2 phase, the element-specific bond length variations follow the relation $\sigma^2_{\text{In-Se}} < \sigma^2_{\text{Ga-Se}} < \sigma^2_{\text{Cu-Se}}$ for all Cu/III ratios between 0.8 and 1.0. Furthermore, the Ga-Se and In-Se bond length variations increase with decreasing Cu content while $\sigma^2_{\text{Cu-Se}}$ remains constant within the uncertainty for all Cu/III ratios. For the 1-3-5 and 1-5-8 phase, the increase of the Ga-Se and In-Se bond length variations with decreasing Cu content observed for the 1-1-2 phase is continued to Cu/III = 0.34 and Cu/III = 0.22 with basically the same slope corresponding to an increase of 65 to 80 % for the 1-5-8 phase compared to the stoichiometric 1-1-2 phase. The Cu-Se bond length variation is similar for the 1-3-5 and 1-5-8 phase and is only slightly larger than $\sigma^2_{\text{Cu-Se}}$ for the 1-1-2 phase, corresponding to an increase of approximately 15 %.[2]

The bond length variation originates from thermal vibrations of the atoms relative to each other, even at low temperature, and from static variations due to defects, different local configurations, or lattice distortions. The thermal contribution can be estimated using a correlated Einstein model, which contains the reduced mass μ of the atomic pair and the bond stretching force constant $k^{||}$ as characteristic parameters [40,42]. For a given temperature, an increase in μ or $k^{||}$ leads to a decrease of σ^2. For the 1-1-2 phase, the bond stretching force constant of the Cu-Se bond is significantly smaller than those of the Ga-Se and In-Se bonds [30,31,46] while the reduced mass of the In-Se pair is significantly larger than those of the Cu-Se and Ga-Se pairs. Therefore, the thermal contribution to σ^2 follows the relation In-Se < Ga-Se < Cu-Se at low temperatures [33]. Similarly, a softer bond will respond more to stress and strain created by defects and lattice distortions than a stiffer bond. A larger static bond length variation is thus expected for bonds with smaller bond stretching force constant [33]. Furthermore, a larger amount of Ga related defects than In related defects can be assumed for the 1-1-2 phase given the difference in radii and bond lengths of Cu and Ga compared to In [34]. Therefore, the static contribution to σ^2 is also expected to follow the relation In-Se < Ga-

[2] Note that a linear increase of $\sigma^2_{\text{Cu-Se}}$ from Cu/III = 1.0 to Cu/III = 0.22 would also be consistent with the data within the uncertainty.

Se < Cu-Se. The relation $\sigma^2_{In\text{-}Se} < \sigma^2_{Ga\text{-}Se} < \sigma^2_{Cu\text{-}Se}$ observed in Fig. 8 for $0.8 \leq Cu/III \leq 1.0$ thus originates from the differences in the reduced mass of the atomic pairs, the strength of the bonds, and potentially the nature and amount of defects in the 1-1-2 phase.

Interestingly, the Ga-Se and In-Se bond length variations strongly increase with decreasing Cu content for all three phases while the Cu-Se bond length variation remains nearly constant. With decreasing Cu/III ratio in the 1-1-2 phase, the number of Cu vacancies and In on Cu antisites (and presumably Ga on Cu antisites) increases. However, this does not directly affect the Cu-Se bond length distribution since no Cu atoms are involved in these point defects. Furthermore, theoretical calculations have shown only one Cu-Se distance for $CuIn_5Se_8$ consistent with the fact that Cu is contained only in the $\kappa = 7$ configuration [19,24,28]. The static contribution to the Cu-Se bond length variation can thus be expected to be similar for all three phases. The small increase of $\sigma^2_{Cu\text{-}Se}$ by about 15 % for the 1-3-5 and 1-5-8 phases compared to the 1-1-2 phase most likely stems from an increase of the thermal vibrations facilitated by the large amount of vacancies present in the structure as discussed above. In contrast, the number of different local configurations involving In and Ga atoms significantly increases with decreasing Cu/III ratio and thus an increasing static variation of the Ga-Se and In-Se bond lengths can be expected. In fact, theoretical studies of $CuIn_5Se_8$ observe strong variations in the bond lengths of the different In-Se pairs contained in the $\kappa = 7$ and $\kappa = 9$ configurations [19,24,28]. The strong increase of $\sigma^2_{In\text{-}Se}$ and presumably also of $\sigma^2_{Ga\text{-}Se}$ with decreasing Cu/III is thus mostly caused by an increase of the static bond length variation due to an increasing number of local atomic configurations in Cu-poor $Cu(In,Ga)Se_2$ as well as $Cu(In,Ga)_3Se_5$ and $Cu(In,Ga)_5Se_8$.

5. Conclusions

Element-specific average bond lengths and bond length variations were determined for the Cu-Se, Ga-Se, and In-Se bonds of $Cu(In,Ga)_3Se_5$ and $Cu(In,Ga)_5Se_8$ alloys using low-temperature EXAFS measurements. The results are compared to those of a similar study previously conducted for $Cu(In,Ga)Se_2$ alloys. For all three series, the average Cu-Se and Ga-Se bond lengths are nearly identical whereas the average In-Se bond length is significantly larger, despite the fact that Ga and In share the same lattice site. Furthermore, the average Cu-Se, Ga-Se, and In-Se bond lengths exhibit a small increase with increasing In/III ratio, however, the change is about one order of magnitude less than the corresponding increase of the unit cell dimensions. The present study therefore demonstrates that alloying of In and Ga

leads to the same bond length behavior in all three Cu-(In,Ga)-Se series irrespective of the Cu/III ratio.

Comparing the structural parameters as a function of the Cu content, a significant decrease of the unit cell volume for decreasing Cu/III ratio was observed in the literature. In contrast, the element-specific average bond lengths obtained from the extensive set of samples in this study clearly exhibit a slight increase with decreasing Cu/III ratio. This can be understood in terms of the strongly increasing number of cation vacancies in the structure. While the decreasing number of atoms within the unit cell leads to a shrinking of the unit cell, the under-coordination of the Se anions results in a weakening of the bonds and hence in a slight bond length expansion. The vacancies thus affect the long- and short-range structure in a rather different manner.

Both, alloying of In and Ga and changing the Cu/III stoichiometry lead to significant changes of the lattice constants and to mixed occupations of the cation lattice sites. The latter results in different local cation configurations involving various arrangements of Cu, Ga, In, and vacancies. Interestingly, this study shows that the element-specific average bond lengths remain almost the same independent of composition and stoichiometry and only the bond length variations increase with decreasing Cu content. This trend of bond length conservation originates from the fact that a change of the bond lengths requires significantly more energy than a change of the bond angles. As a consequence, the Se anion relaxes to a position that keeps bond length distortions to a minimum. The position of one particular Se anion therefore depends on the individual configuration of neighboring cations and is typically different from the average Se position given by the crystal structure. Furthermore, the distance between two lattice sites is different from the element-specific bond lengths if one of the lattice sites features a mixed site occupation. However, it can be expressed as the average over different element-specific bond lengths weighted by the corresponding site occupation factors. Comparing element-specific bond lengths obtained from EXAFS and lattice site distances obtained from diffraction thus provides a powerful method to verify the site occupation factors in multinary compounds and alloys, as demonstrated in this work.

For $Cu(In,Ga)Se_2$, $Cu(In,Ga)_3Se_5$, and $Cu(In,Ga)_5Se_8$ alloys, the crystallographic long-range structure and the element-specific short-range structure therefore describe different structural aspects that are clearly interrelated but not identical. For a comprehensive understanding of these material systems both aspects must be considered since the electronic states and thus important material properties are affected by the crystallographic long-range structure and by the element-specific short-range structure.

ACCEPTED MANUSCRIPT

Acknowledgements

We acknowledge the ESRF and the CNR-IOM for provision of synchrotron radiation facilities during the HC-1284 experiment. We further thank Yvonne Tomm for her contribution in the material synthesis, Christian Wolf for the ICP-MS analysis of selected samples, and Giordano Montegrossi (CNR-IGG) for experimental support during the synchrotron beamtime. This work was funded by the ESRF, the German Federal Ministry for Economic Affairs and Energy under the “comCIGS-II” and “speedCIGS” projects [Grant No. 0325448E and 0324095E], the Friedrich-Schiller-Universität Jena under the ProChance Initiative [Grant No. 2.11.3-A1/2012-01], and the Department of Earth Sciences of the University of Florence under the ex-60% programme.

ACCEPTED MANUSCRIPT

References

[1] P. Jackson, R. Wuerz, D. Hariskos, E. Lotter, W. Witte, M. Powalla, Effects of heavy alkali elements in Cu(In,Ga)Se_2 solar cells with efficiencies up to 22.6%, Phys. Stat. Sol. RRL 10 (2016) 583-586.

[2] H. Rodriguez-Alvarez, A. Weber, J. Lauche, C.A. Kaufmann, T. Rissom, D. Greiner, M. Klaus, T. Unold, C. Genzel, H.-W. Schock, R. Mainz, Formation of $CuInSe_2$ and $CuGaSe_2$ Thin Films Deposited by Three-Stage Thermal Co-Evaporation: A Real-Time X-Ray Diffraction and Fluorescence Study, Adv. Energy Mater. 3 (2013) 1381-1387.

[3] P. Pistor, S. Zahedi-Azad, S. Hartnauer, L.A. Wägele, E. Jarzembowski, R. Scheer, Real time observation of phase formations by XRD during Ga-rich or In-rich Cu(In,Ga)Se_2 growth by co-evaporation, Phys. Stat. Sol. A 212 (2015) 1897-1904.

[4] C. Stephan, S. Schorr, M. Tovar, H.-W. Schock, Comprehensive insights into point defect and defect cluster formation in $CuInSe_2$, Appl. Phys. Lett. 98 (2011) 091906.

[5] C. Stephan, T. Scherb, C. A. Kaufmann, S. Schorr, H.-W. Schock, Cationic point defects in $CuGaSe_2$ from a structural perspective, Appl. Phys. Lett. 101 (2012) 101907.

[6] C. Stephan, D. Greiner, S. Schorr, C.A. Kaufmann, The influence of sodium on the point defect characteristics in off stoichiometric $CuInSe_2$, J. Phys. Chem. Solids 98 (2016) 309-315.

[7] H.W. Spiess, U. Haeberlen, G. Brandt, A. Räuber, J. Schneider, Nuclear Magnetic-Resonance in I-III-VI_2 Semiconductors, Phys. Stat. Sol. B 62 (1974) 183-192.

[8] D.K. Suri, K.C. Nagpal, G.K. Chadha, X-Ray Study of $CuGa_xIn_{1-x}Se_2$ Solid-Solutions, J. Appl. Crystallogr. 22 (1989) 578-583.

[9] T. Tinoco, C. Rincon, M. Quintero, G.S. Perez, Phase-diagram and optical-energy gaps for $CuIn_yGa_{1-Y}Se_2$ alloys, Phys. Stat. Sol. A 124 (1991) 427-434.

[10] M. Souilah, A. Lafond, C. Guillot-Deudon, S. Harel, M. Evain, Structural investigation of the Cu_2Se-In_2Se_3-Ga_2Se_3 phase diagram, X-ray photoemission and optical properties of the $Cu_{1-z}(In_{0.5}Ga_{0.5})_{1+\,z/3}Se_2$ compounds, J. Solid State Chem. 183 (2010) 2274-2280.

[11] W. Hönle, G. Kühn, U.C. Boehnke, Crystal structures of two quenched Cu-In-Se phases, Cryst. Res. Technol. 23 (1988) 1347-1354.

[12] G. Marin, S. Tauleigne, S.M. Wasim, R. Guevara, J.M. Delgado, C. Rincon, A.E. Mora, G.S. Perez, X-ray powder diffraction and optical characterization of the $Cu(In_{1-x}Ga_x)_3Se_5$ semiconducting system, Mater. Res. Bull. 33 (1998) 1057-1068.

[13] J.M. Merino, S. Mahanty, M. Leon, R. Diaz, F. Rueda, J.L. Martin de Vidales, Structural characterization of $CuIn_2Se_{3.5}$, $CuIn_3Se_5$ and $CuIn_5Se_8$ compounds, Thin Solid Films, 361-362 (2000) 70-73.

[14] T. Hanada, A. Yamana, Y. Nakamura, O. Nittono, T. Wada, Crystal structure of $CuIn_3Se_5$ semiconductor studied using electron and X-ray diffractions, Jpn. J. Appl. Phys. 36 (1997) L1494-L1497.

[15] W. Paszkowicz, R. Lewandowska, R. Bacewicz, Rietveld refinement for $CuInSe_2$ and $CuIn_3Se_5$, J. Alloys Compd. 362 (2004) 241-247.

[16] S. Lehmann, D.F. Marron, M. Tovar, Y. Tomm, C. Wolf, S. Schorr, T. Schedel-Niedrig, E. Arushanov, M.C. Lux-Steiner, A structural study on the $CuGaSe_2$-related copper-poor materials $CuGa_3Se_5$ and $CuGa_5Se_8$: thin-film vs. bulk material, Phys. Stat. Sol. A 206 (2009) 1009-1012.

[17] S. Lehmann, D.F. Marron, M. Leon, R. Feyerherm, E. Dudzik, E.J. Friedrich, M. Tovar, Y. Tomm, C. Wolf, S. Schorr, T. Schedel-Niedrig, M.C. Lux-Steiner, J.M. Merino, Long-range structure of $Cu(In_xGa_{1-x})_3Se_5$: A complementary neutron and anomalous x-ray diffraction study, J. Appl. Phys. 109 (2011) 013518.

[18] S. Yamazoe, H. Kou, T. Wada, A structural study of Cu-In-Se compounds by x-ray absorption fine structure, J. Mater. Res. 26 (2011) 1504-1516.

[19] T. Maeda, W. Gong, T. Wada, Crystallographic and optical properties and band structures of $CuInSe_2$, $CuIn_3Se_5$, and $CuIn_5Se_8$ phases in Cu-poor Cu_2Se–In_2Se_3 pseudo-binary system, Jpn. J. Appl. Phys. 55 (2016) 04ES15.

[20] L. Duran, S.M. Wasim, C.A.D. Rincon, E. Hernandez, C. Rincon, J.M. Delgado, J. Castro, J. Contreras, Growth, structural characterization, and optical band gap of $Cu(In_{1-x}Ga_x)_5Se_8$ alloys, Phys. Stat. Sol. A 199 (2003) 220-226.

[21] S.B. Zhang, S.-H. Wei, A. Zunger, Stabilization of ternary compounds via ordered arrays of defect pairs, Phys. Rev. Lett. 78 (1997) 4059-4062.

[22] S.B. Zhang, S.-H. Wei, A. Zunger, H. Katayama-Yoshida, Defect physics of the $CuInSe_2$ chalcopyrite semiconductor, Phys. Rev. B 57 (1998) 9642-9656.

[23] R. Lewandowska, R. Bacewicz, J. Filipowicz, EXAFS study of In-rich phases in Cu-In-Se system, Cryst. Res. Technol. 37 (2002) 235-241.

[24] C.-H. Chang, S.-H. Wei, J.W. Johnson, S.B. Zhang, N. Leyarovska, G. Bunker, T.J. Anderson, Local structure of $CuIn_3Se_5$: X-ray absorption fine structure study and first-principles calculations, Phys. Rev. B 68 (2003) 054108.

[25] J.M. Merino, S. Diaz-Moreno, G. Subias, M. Leon, A comparative study of Cu–Se and In–Se bond length distributions in $CuInSe_2$ with related In-rich compounds, Thin Solid Films 480–481 (2005) 295-300.

[26] M. Leon, J.M. Merino, E. Arushanov, Comparative study of structural and optical parameters of $CuInSe_2$ and various $CuIn_xSe_y$ compounds, Moldavian J. Phys. Sci. 5 (2006) 373-381.

[27] A. Wolska, R. Bacewicz, J. Filipowicz, K. Attenkofer, X-ray absorption near-edge structure of selenium in the Cu-In-Se system, J. Phys.: Condes. Matter 13 (2001) 4457-4470.

[28] F. Jiang, J. Feng, First principles calculation on polytypes of ordered defect compound $CuIn_5Se_8$, Appl. Phys. Lett. 89 (2006) 221920.

[29] C.D.R. Ludwig, T. Gruhn, C. Felser, J. Windeln, Defect structures in $CuInSe_2$: A combination of Monte Carlo simulations and density functional theory, Phys. Rev. B 83 (2011) 174112.

[30] C.S. Schnohr, H. Kämmer, C. Stephan, S. Schorr, T. Steinbach, J. Rensberg, Atomic-scale structure and band-gap bowing in $Cu(In,Ga)Se_2$, Phys. Rev. B 85 (2012) 245204.

[31] C.S. Schnohr, Compound semiconductor alloys: From atomic-scale structure to bandgap bowing, Appl. Phys. Rev. 2 (2015) 031304.

[32] R. Sarmiento-Perez, S. Botti, C.S. Schnohr, I. Lauermann, A. Rubio, B. Johnson, Local versus global electronic properties of chalcopyrite alloys: X-ray absorption spectroscopy and ab initio calculations, J. Appl. Phys. 116 (2014) 093703.

[33] C.S. Schnohr, H. Kämmer, T. Steinbach, M. Gnauck, T. Rissom, C.A. Kaufmann, C. Stephan, S. Schorr, Composition-dependent nanostructure of $Cu(In,Ga)Se_2$ powders and thin films, Thin Solid Films 582 (2015) 356-360.

[34] C.S. Schnohr, S. Eckner, P. Schöppe, E. Haubold, F. d'Acapito, D. Greiner, C.A. Kaufmann, Reversible correlation between subnanoscale structure and Cu content in co-evaporated $Cu(In,Ga)Se_2$ thin films, Acta Mater. 153 (2018) 8-14.

[35] C. Stephan, Structural trends in off stoichiometric chalcopyrite type compound semiconductors, Ph.D. thesis, Freie Universität Berlin/Helmholtz-Zentrum Berlin, Germany (2011). http://dx.doi.org/10.5442/d0011.

[36] F. d'Acapito, S. Colonna, S. Pascarelli, G. Antonioli, A. Balerna, A. Bazzini, F. Boscherini, F. Campolungo, G. Chini, G. Dalba, G. I. Davoli, P. Fornasini, R. Graziola, G. Licheri, C. Meneghini, F. Rocca, L. Sangiogio, V. Sciarra, V. Tullio, S. Mobilio, ESRF Newsletters 30 (1998) 42.

[37] M. Newville, IFEFFIT: interactive XAFS analysis and FEFF fitting, J. Synchrotron Radiat. 8 (2001) 322-324.

[38] B. Ravel, M. Newville, ATHENA, ARTEMIS, HEPHAESTUS: data analysis for X-ray absorption spectroscopy using IFEFFIT, J. Synchrotron Radiat. 12 (2005) 537-541.

[39] J.J. Rehr, J.J. Kas, F.D. Vila, M.P. Prange, K. Jorissen, Parameter-free calculations of X-ray spectra with FEFF9, Phys. Chem. Chem. Phys. 12 (2010) 5503-5513.

[40] P. Fornasini, R. Grisenti, On EXAFS Debye-Waller factor and recent advances, J. Synchrotron Radiat. 22 (2015) 1242-1257.

[41] P. Fornasini, R. Grisenti, M. Dapiaggi, G. Agostini, T. Miyanaga, Nearest-neighbour distribution of distances in crystals from extended X-ray absorption fine structure, J. Chem. Phys. 147 (2017) 044503.

[42] C.S. Schnohr, P. Kluth, L.L. Araujo, D. Sprouster, A.P. Byrne, G.J. Foran, M.C. Ridgway, Anisotropic vibrations in crystalline and amorphous InP, Phys. Rev. B 79 (2009) 195203.

[43] C.A.D. Rincon, E. Hernandez, M.I. Alonso, M. Garriga, S.M. Wasim, C. Rincon, M. Leon, Optical transitions near the band edge in bulk $CuIn_xGa_{1-x}Se_2$ from ellipsometric measurements, Mater. Chem. Phys. 70 (2001) 300-304.

[44] L.E. Oikkonen, M.G. Ganchenkova, A.P. Seitsonen, R.M. Nieminen, Vacancies in $CuInSe_2$: new insights from hybrid-functional calculations, J. Phys.: Condes. Matter 23 (2011) 422202.

[45] S.-H. Wei, A. Zunger, I.-H. Choi, P.Y. Yu, Trends in band-gap pressure coefficients in chalcopyrite semiconductors, Phys. Rev. B 58 (1998) R1710-R1713.

[46] S. Eckner, H. Kämmer, T. Steinbach, M. Gnauck, A. Johannes, C. Stephan, S. Schorr, C.S. Schnohr, Atomic-scale structure, cation distribution, and bandgap bowing in $Cu(In,Ga)S_2$ and $Cu(In,Ga)Se_2$, Appl. Phys. Lett. 103 (2013) 081905.

ACCEPTED MANUSCRIPT

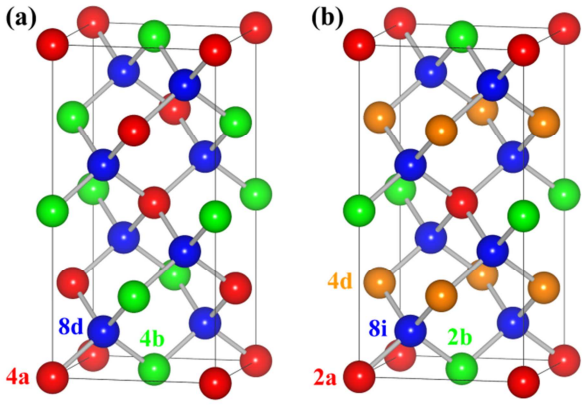

Fig. 1: Schematic of (a) the chalcopyrite type and (b) the stannite type crystal structure.

ACCEPTED MANUSCRIPT

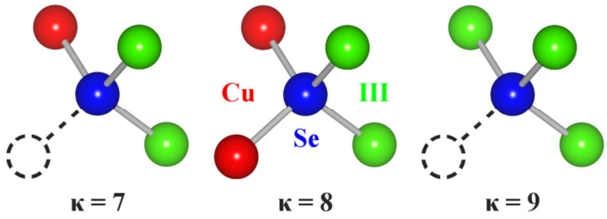

Fig. 2: Schematic of the different local cation configurations, where κ denotes the number of valence electrons. In the alloys, each group III atom can be either In or Ga leading to three different κ = 7 configurations, three different κ = 8 configurations, and four different κ = 9 configurations [29,30].

ACCEPTED MANUSCRIPT

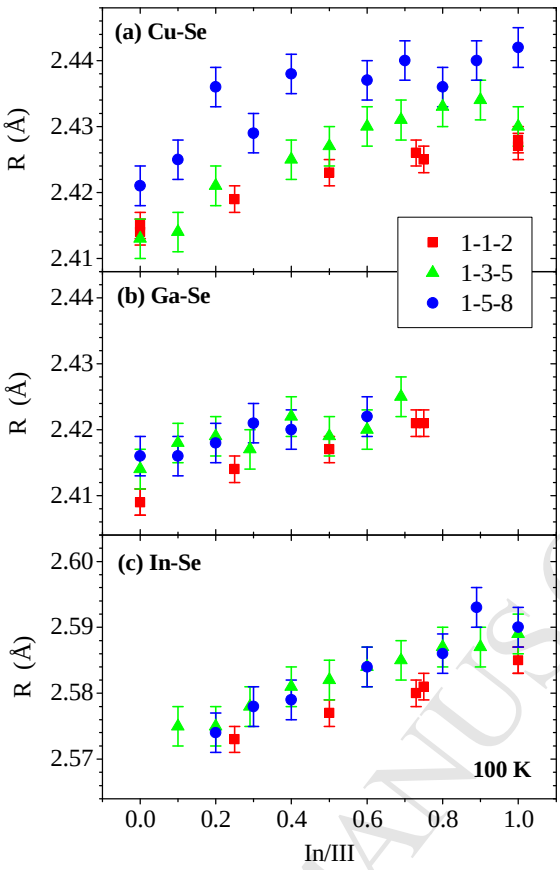

Fig. 3: Average (a) Cu-Se, (b) Ga-Se, and (c) In-Se bond length R as a function of the In/III ratio for $Cu(In,Ga)Se_2$ (1-1-2, red squares), $Cu(In,Ga)_3Se_5$ (1-3-5, green triangles), and $Cu(In,Ga)_5Se_8$ (1-5-8, blue circles) at 100 K. The data for the 1-1-2 phase were originally measured at 17 K [33] and have been adjusted to a temperature of 100 K as described in Sect. 2.3.

ACCEPTED MANUSCRIPT

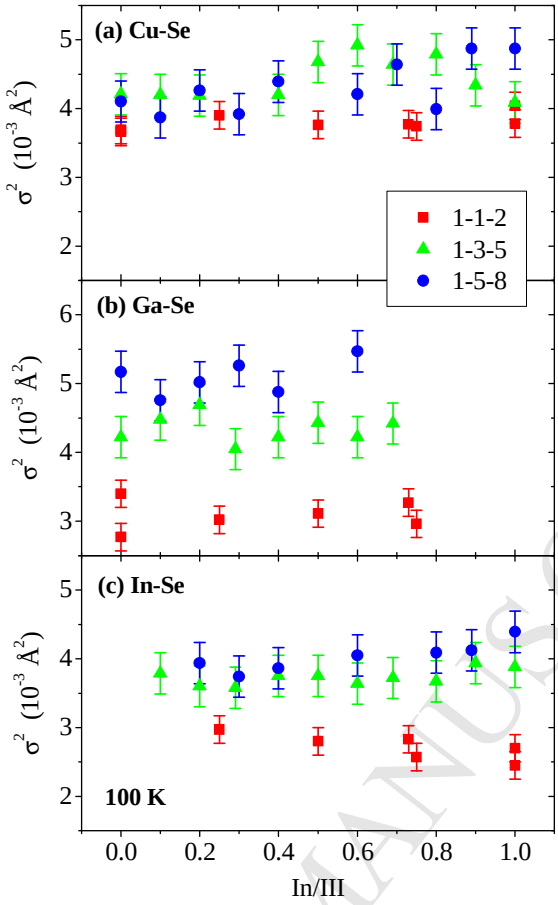

Fig. 4: (a) Cu-Se, (b) Ga-Se, and (c) In-Se bond length variation σ^2 as a function of the In/III ratio for $Cu(In,Ga)Se_2$ (1-1-2, red squares), $Cu(In,Ga)_3Se_5$ (1-3-5, green triangles), and $Cu(In,Ga)_5Se_8$ (1-5-8, blue circles) at 100 K. The data for the 1-1-2 phase were originally measured at 17 K [33] and have been adjusted to a temperature of 100 K as described in Sect. 2.3.

ACCEPTED MANUSCRIPT

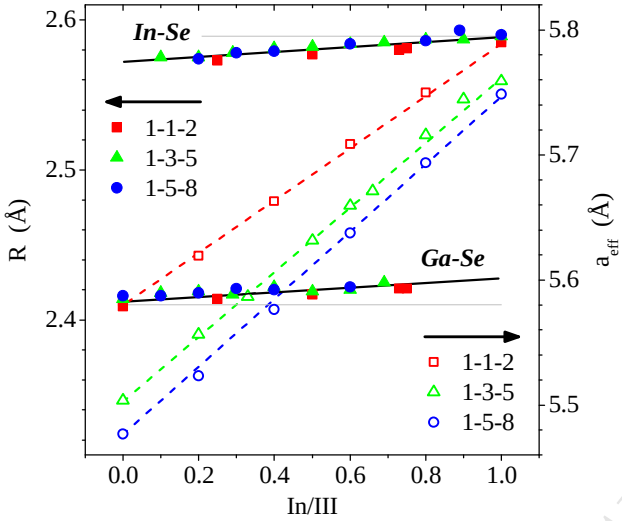

Fig. 5: Comparison of the average Ga-Se and In-Se bond lengths (full symbols, left scale) as a function of In/III ratio for Cu(In,Ga)Se_2 (1-1-2, red squares), Cu(In,Ga)$_3Se_5$ (1-3-5, green triangles), and Cu(In,Ga)$_5Se_8$ (1-5-8, blue circles). The data for the 1-1-2 phase are calculated from [33] as described in Sect. 2.3. On this scale, the uncertainty of the data is smaller than the size of the symbols. Additionally, the effective lattice constant a_{eff} (open symbols, right scale) is plotted for the 1-1-2 phase as calculated from [43], for the 1-3-5 phase as calculated from [17], and for the 1-5-8 phase as calculated from [20]. The effective lattice constant is defined by $V = a^2c = 2a_{eff}^3$, where a and c denote the tetragonal lattice constants and V represents the unit cell volume. All lines are a guide to the eye.

ACCEPTED MANUSCRIPT

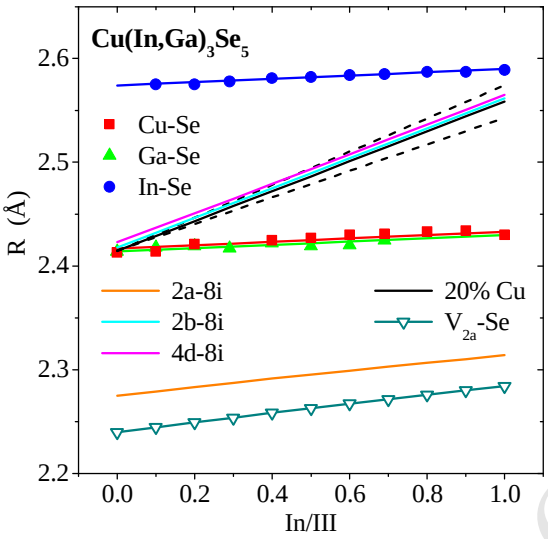

Fig. 6: Comparison of the element-specific average Cu-Se, Ga-Se, and In-Se bond lengths determined by EXAFS (full symbols and lines) and the distance between the 2a and 8i, 2b and 8i, and 4d and 8i crystallographic lattice sites determined by neutron diffraction [17] (colored solid lines) for $Cu(In,Ga)_3Se_5$. The calculated vacancy bond length (distance between a vacancy on the 2a site and the neighboring Se anions, open symbols and line) and the calculated distance between a cation lattice site occupied by 20% Cu, 80% In or Ga and the 8i site (black solid line) are also shown. The calculated distance between a cation lattice site occupied by 10% Cu, 90% In or Ga or by 30% Cu, 70% In or Ga and the 8i site (black dashed lines) are plotted for comparison.

ACCEPTED MANUSCRIPT

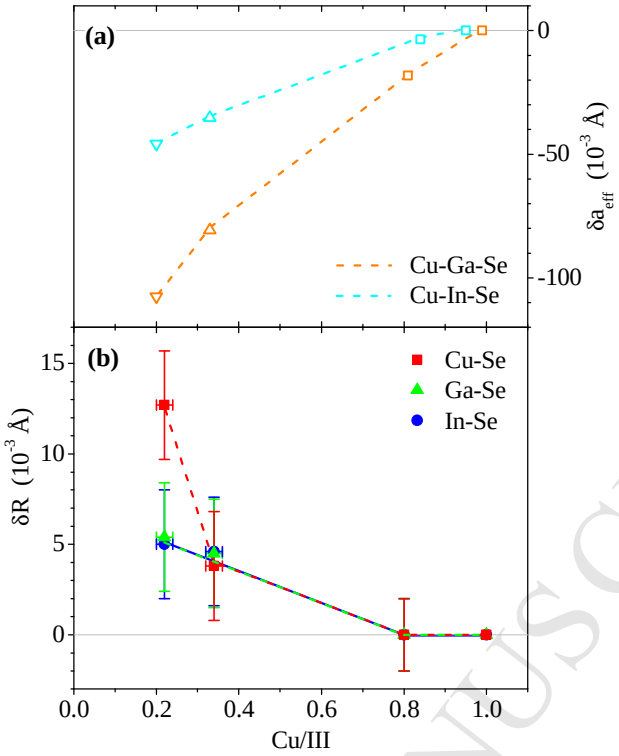

Fig. 7: (a) Crystal structure contraction $\delta a_{eff} = a_{eff}(Cu/III) - a_{eff}(Cu/III=1.00)$ for the pure Cu-Ga-Se and Cu-In-Se systems (open symbols, right scale) as a function of the Cu/III ratio and (b) local bond length expansion $\delta R = R(Cu/III) - R(Cu/III=1.00)$ for Cu-Se, Ga-Se, and In-Se bonds (full symbols, left scale). The data in (a) are taken from [17,20,35]. The lines are a guide to the eye. Note the different scales in panels (a) and (b).

ACCEPTED MANUSCRIPT

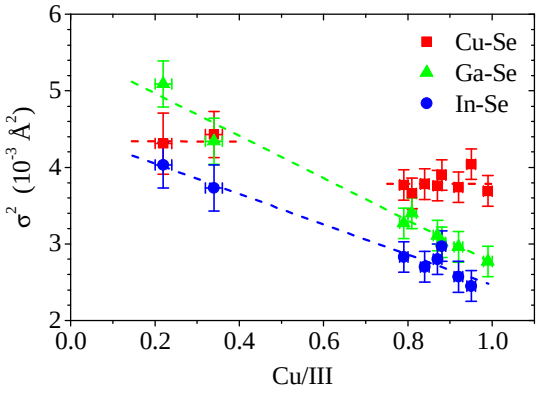

Fig. 8: Comparison of the Cu-Se (red squares), Ga-Se (green triangles), and In-Se (blue circles) bond length variations as a function of Cu/III ratio. The data for the 1-1-2 phase with $0.8 \leq$ Cu/III ≤ 1.0 are calculated from Ref. [33] as described in the text. For Ga-Se and In-Se, the lines represent linear fits to the data. For Cu-Se, the lines are a guide to the eye.

ACCEPTED MANUSCRIPT

ACCEPTED MANUSCRIPT

Highlights **"Short-range versus long-range structure in $Cu(In,Ga)Se_2$, $Cu(In,Ga)_3Se_5$, and $Cu(In,Ga)_5Se_8$"**

Haubold et al.

- Lattice constants increase with increasing In/Ga ratio and Cu content.
- In contrast, element-specific average bond lengths remain nearly constant.
- Vacancies lead to unit cell contraction but slight bond length expansion.
- Lattice site distances deviate from element-specific bond lengths for most sites.
- Atomic short-range structure differs from crystallographic long-range structure.

ACCEPTED MANUSCRIPT